Numerical Simulation of Lead-Free Bismuth-Based Perovskite Solar Cell with Addition of an Interface Layer between Absorber Layer and Electron Transport Layer

[1*]Srishti Shashi and [2]Dr. Rajnish Bhasker

Corresponding author: Srishti Shashi
Address: [1*]Department of Electrical Engineering, Power System, Veer Bahadur Singh Purvanchal University, Jaunpur, Uttar Pradesh, India; [2]Department of Electrical Engineering, Veer Bahadur Singh Purvanchal University, Jaunpur, Uttar Pradesh, India
E-mail: [1*]srishtishashi8@gmail.com; [2]raj_b33@rediffmail.com

Abstract

In terms of affordability and improved power conversion efficiency (PCE), lead-based Perovskite Solar Cells have significantly outperformed silicon-based solar cells. Lead-based PSCs still have difficulties with regard to commercialization due to lead toxicity and stability problems. Therefore, a lead-free bismuth-based perovskite absorber layer was examined in this research effort using TiO_2 as electron transport layer (ETL) and Cu_2O as hole transport layer (HTL). Thus, the proposed device structure Au/Cu_2O/$Cs_3Bi_2I_9$/TiO_2/TCO is being numerically investigated with SCAPS-1D software. Which shows 14.20% of PCE. For practical consideration, including defects, the proposed structure is simulated. Moreover, to enhance the PCE of the proposed device structure, an interface layer of n-3C-SiC was inserted between the absorber layer and ETL, giving 15.03% of power conversion efficiency. This demonstrates an improvement in the PCE of the suggested device structure of 0.83%. The investigation of each layer's thickness and doping density is further optimized. The maximum PCE is up to 15.63% for modified structure in order to attain the greatest PCE of device structure showing. So, these results will be helpful to a better understanding of the bismuth-based PSC with an interface layer.

Key Words: Lead free perovskite solar cell, numerical simulation, Cu_2O, $Cs_3Bi_2I_9$, n-3C-SiC, TiO_2, SCAPS-1D.

DOI Number: 10.48047/nq.2022.20.19.NQ99048 **NeuroQuantology2022; 20(19):524-534**

1 Introduction

The electricity demand has continuously increasing day by day globally. To fulfill all those electricity demands, reliable, affordable clean, and sustainable energy sources are required. However, with the help of coal, oils, and solid biomass fuel, more than 80% of energy demand is fulfilled in India only. Thus, demand for fossil fuels is still increasing continuously in future. For that, fossil fuels are not enough alone. That indicates, Meet such huge energy demand with energy generation, renewable energy sources can be the only replacements. Solar energy is playing a vital role in the energy sector because of its high stability and eco-friendly solution. But instead of that, existing silicon-based solar cells are even costlier today. It creates an interesting angle for the research scholars toward the design analysis of cost-effective solar cells. Recently, thin film solar technology has become competitive because of its solution processability, low cost and high efficiency. Perovskite has ABX_3 formula, where A is an organic or inorganic cation such as Methylammonium (MA), Ethylammonium (EA), or Formamidinium (FA). B is a divalent metal

ion such as Lead (Pb), Tin (Sn), Germanium (Ge) and X_3 is a halide anion such as Br^-, Cl^-, or I^- [1]. As of 2022, Lead-based perovskite solar cells have attained more than 25% of PCE [2]. However, because to the hazardous ingredient lead (Pb) and stability problems, lead-based PSCs are still a long way from being commercially viable. The toxicity of lead can be overcome by applying any of the strategies. The first one is to replace Lead (Pb) by its substitutes available in the periodic table having similar properties. And next, the second one is by making the perovskite absorber layer free from lead material [3]. So, analysis and development of Lead-free perovskite absorbing layers could be the best alternatives for it [4], [5].

The structural formula for Bi-based halide perovskite is $A_3Bi_2X_9$, where A denotes monovalent cation (Na^+, K^+, Rb^+, Cs^+ or $CH_3NH_3^+$) and X denotes halogen atom (F, Cl, Br, or I) [6]. Bismuth-based PSC structure, AZO/c-TiO_2/$Cs_3Bi_2I_9$/CuSCN/graphite solar cell shows a very low PCE of 0.17%. Due to the poor thin film morphology of the Bi-based perovskite solar cell fabricated through the conventional spin coating method, a 1.64% PCE was reported, but in the recent paper, it achieved up to the highest PCE of 3.20% [7], [8] and [9]. Performance parameters of the PSC do not depend only on the variation of thickness, temperature, doping concentration, and band gap, But it depends on the defect density of states (DOS) in cell structure. Due to defects, the DOS performance of the solar cell degrades. Thus, more study should be done regarding defect tolerance in the cell structure. By changing the defect density of states, characteristic decay energy, and capture cross-section area of trap, it was theoretically possible to examine the structure ITO/PEDOT: PSS/$MAGeI_3$/PCBM/Au, which demonstrates a decline in the cell performances [10].

Perovskite devices can utilize different types of electron transport materials (ETMs) and hole transport materials (HTMs) for lead-based and lead-free perovskite solar cell were studied by many researchers earlier. TiO_2 and Spiro-OME-TAD are most famous electron transport material and hole transport material respectively. Spiro-OME-TAD, PEDOT: PSS, P3HT, Cu_2O, CuI, PTAA, CuSCN, CuO, and NiO can be used as different HTMs. Other materials like ZnO, PCBM, IGZO, TiO_2, ZnSe, SnO_2, CdS, and ZnOS can be used as different ETMs [11], [12] and [13].

In this study, the proposed cell structure's performance metrics were first compared with and without defects. In order to improve the PCE of the proposed device structure, an interface layer was also placed between the absorber layer and the electron transport layer. Then this modified device structure will be simulated further, with and without defects. Moreover, a detailed and more practical simulation analysis of the modified device structure having defects will investigate. In the improved device structure, which was simulated using the SCAPS simulator, efficiency was optimized for the variation in each layer's thickness and doping density.

2 Device Structure and Methodology

In this work, the proposed structure Au/Cu_2O/$Cs_3Bi_2I_9$/TiO_2/TCO is shown in Figure 1(a), where a bismuth-based lead-free perovskite absorber layer is sandwiched between Cu_2O as HTL and TiO_2 as ETL. Gold (Au) and transparent thin conductive oxide (TCO) are the back and front metal contacts, respectively. An interfacial layer n-3C-SiC was inserted between the absorber and ETL layer to enhance the PCE of the proposed cell. Hence, the modified structure Au/Cu_2O/$Cs_3Bi_2I_9$/n-3C-SiC/TiO_2/TCO is depicted in Figure 1(b) along with its energy band diagram is in Figure 1(c). for numerical simulation analysis of PSCs by using SCAPS-1D, all required electrical and optical parameters of the materials taken from the previous papers, which listed in **Table 2** [14], [15] and [11]. The simulation analysis of the proposed structure will be divided into three parts. First, the proposed structure Au/Cu_2O/$Cs_3Bi_2I_9$/TiO_2/TCO will be investigated without and with defect having the value N_t = 0/cm^3 and 1×10^{15}/cm^3 respectively. Second, To enhance the PCE of the proposed structure, An interface layer will be introduced between the absorber layer and ETL. The newly modified structure will be analyzed, further without and with defects having N_t = 0/cm^3 and 1×10^{15}/cm^3, respectively. Third, for more detailed and practical simulation results, the newly modified structure having defects are investigated with respect to the thickness variation and doping concentration variation on each layer, To calculate the electrical performance parameters of the cell structure, like open circuit voltage (V_{oc}), short circuit current density (J_{sc}) Fill-factor (FF) and PCE (eta). The optimized thickness and doping density of each layer will be placed in the redesigned cell structure, and then the optimized performance characteristics of the modified structure will be determined.

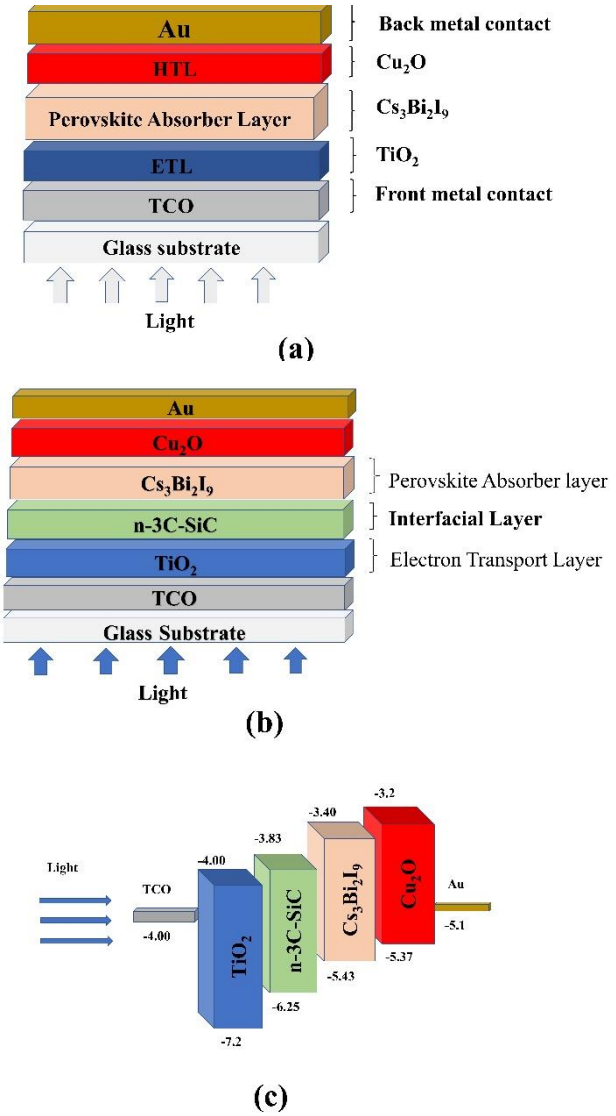

Figure 1: (a) Device structure of proposed PSC (b) Modified schematic diagram and (c) Energy band diagram of lead-free bismuth-based PSC ($Au/Cu_2O/Cs_3Bi_2I_9/n$-3C-SiC/TiO_2)

3 Simulation, Modelling and Design Parameters

For the numerical simulation study of the solar cell, SCAPS-1D (Solar Cell Capacitance Simulator-One Dimensional) software version 3.3.10 is used in this study, Which was developed by Electronics and Information System (ELIS), University of Gent, Belgium [16]. It utilizes four different sets of Photo Voltaic (PV) equations, one for each carrier density for electrons and holes [17]. Which are:

1) Poisson equation:

$$\frac{d^2\varphi(x)}{dx^2} = \frac{e}{\varepsilon_0\varepsilon_r}\left(p(x) - n(x) + N_D + N_A + \rho_p - \rho_n\right) \quad (1)$$

2) Continuity equation:

$$\frac{dJ_n}{dx} = Gr - Rr \quad (2)$$

$$\frac{dJ_p}{dx} = Gr - Rr \quad (3)$$

3) Charge transport equation:

$$J_n = D_n\frac{dn}{dx} + \mu_n n\frac{d\varphi}{dx} \quad (4)$$

$$J_p = D_p\frac{dp}{dx} + \mu_P p\frac{d\varphi}{dx} \quad (5)$$

4) Absorption coefficient equation:

$$\alpha(\lambda) = \left(A + \frac{B}{h\nu}\right)\sqrt{h\nu - E_g} \quad (6)$$

The symbols, which have used in the above equations, along with their definitions, and units listed below in **Table 1**.

Table 1

Definition and unit of used symbols in SCAPS-1D simulator

Symbol	Definition	Units
φ	Electrostatic potential	V
e	Electron charge	C
ε_0	Permittivity of vacuum	F/cm
ε_r	Relative permittivity	
p(x)	Hole density as a function of x	cm^{-3}
n(x)	Electron density as a function of x	cm^{-3}
N_D	Shallow donor impurity density	cm^{-3}
N_A	Shallow acceptor impurity density	cm^{-3}
ρ_p	Hole density distribution	cm^{-3}
ρ_n	Electron density distribution	cm^{-3}
J_n	Electron current density	A/cm^2
J_p	Hole current density	A/cm^2
Gr	Generation rate	$cm^{-3}s^{-1}$
Rr	Recombination rate	$cm^{-3}s^{-1}$
D_n	Diffusion coefficient of electron	cm^2/s

eISSN 1303-5150

D_p	Diffusion coefficient of hole	cm^2/s
μ_n	Mobility of electron	cm^2/Vs
μ_p	Mobility of hole	cm^2/Vs
α	Coefficient of absorption	cm^{-1}
λ	Wavelength	µm
h	Plank constant	Js
v	Frequency of photons	Hz
E_g	Band gap	eV
A, B	Constants	

Moreover, SCAPS-1D software can design and simulate solar cells structure up to seven layers with their front and back metal contacts, and an interface study between any two layers can investigate. Illumination spectrum air mass AM1.5 (1000w/m2) and 300K working temperature are used for the presented numerical simulation study. Material parameters of the cell structure required by SCAPS-1D, are taken from previous literature as listed and cited in **Table 2**.

Table 2
Materials parameters of the lead-free PSCs

PARAMETERS	**Cu_2O**	**$Cs_3Bi_2I_9$**	**n-3C-SiC**	**TiO_2**
Thickness, d (nm)	150	500	30	100
Band gap, E_g (eV)	2.17	2.03	2.42	3.2
Electron affinity, χ (eV)	3.2	3.4	3.83	4.0
Dielectric permittivity, ε_r	7.1	9.68	9.72	9.0
Effective density states at CB, N_c ($/cm^3$)	2.5×10^{18}	4.98×10^{19}	1.553×10^{19}	2×10^{18}
Effective density states at VB, N_v ($/cm^3$)	1.8×10^{19}	2.11×10^{19}	1.163×10^{19}	2×10^{19}
Thermal velocity of electron (cm/s)	1×10^7	1×10^7	1×10^7	1×10^7
Thermal velocity of hole (cm/s)	1×10^7	1×10^7	1×10^7	1×10^7
Mobility of electron, μ_e (cm^2/Vs)	200	4.3	650	0.2
Mobility of hole, μ_h (cm^2/Vs)	80	1.7	40	0.1
Shallow uniform donor density, N_D ($/cm^3$)	0	1×10^9	1×10^{18}	1×10^{19}
Shallow uniform acceptor density, N_A ($/cm^3$)	1×10^{18}	1×10^9	0	0
Radiative recombination coefficient (cm^3/s)	2.3×10^{-9}	2.3×10^{-9}	-	2.3×10^{-9}
Defect density, N_t ($/cm^3$)	1×10^{15}	1×10^{15}	-	1×10^{15}
Reference	[15]	[15]	[14]	[14]

4 Results And Discussion

Simulation analysis of the proposed structure $Au/Cu_2O/Cs_3Bi_2I_9/TiO_2/TCO$ can be divided into three parts discussed below. First, the proposed structure is investigated, without and with defects having N_t = 0 $/cm^3$ and 1×10^{15} $/cm^3$, respectively. Thus, by considering these input parameters one by one, Their simulated performance parameters are listed in **Table 3**.

Table 3
Effect of total defect density in each layer on the performance parameters of the proposed structure $Au/Cu_2O/Cs_3Bi_2I_9/TiO_2/TCO$

Without total defect density (N_t = 0 $/cm^3$)		**With total defect density (N_t = 1×10^{15} $/cm^3$)**	
Eta (%)	14.20	Eta (%)	13.39
V_{oc} (V)	1.48	V_{oc} (V)	1.46
J_{sc} (mA/cm^2)	11.57	J_{sc} (mA/cm^2)	11.56
FF (%)	82.86	FF (%)	78.57

Second, to enhance the power conversion efficiency of the proposed cell structure, an interface layer n-3C-SiC is inserted between the bismuth-based perovskite absorber layer and electron transport layer, which forms a modified structure like Au/Cu_2O/$Cs_3Bi_2I_9$/n-3C-SiC/TiO_2/TCO. For analysis of this structure, first, each layer is defect-free, e.g., $N_t = 0/cm^3$, and second, Each layer has some value of defect densities, e.g., $N_t = 1\times10^{15}/cm^3$. Thus, by considering these two values one by one, their simulated performance parameters are listed in **Table 4**.

Table 4

Effect of total defect density in each layer on the performance parameters of the modified structure Au/Cu_2O/$Cs_3Bi_2I_9$/n-3C-SiC/TiO_2/TCO

Without total defect density (N_t = 0 /cm^3)		**With total defect density ($N_t = 1\times10^{15}/cm^3$)**	
Eta (%)	15.03	Eta (%)	14.22
V_{oc} (V)	1.48	V_{oc} (V)	1.45
J_{sc} (mA/cm^2)	11.64	J_{sc} (mA/cm^2)	11.63
FF (%)	87.06	FF (%)	83.82

Third, for more detailed and practical simulation results, the modified structure defect density ($N_t = 1\times10^{15}/cm^3$) on each layer is optimized. by changing each layer's thickness and doping density to attain maximum PCE of the lead-free perovskite cell structure.

4.1 Thickness Optimization of The Modified Model

4.1.1 Effect of Thickness variation on Absorber Layer ($Cs_3Bi_2I_9$)

To optimize the effect of thickness variation on the absorber layer, within the range of 100nm to 1000nm, the thickness of HTL, interface layer, and ETL is fixed at 150nm, 100nm, and 100nm respectively. Then changes in solar cell's electrical properties like open-circuit voltage, short-circuit current density, Fill-Factor, and power conversion efficiency were observed. Figure 2 makes it clear that PCE (%) and J_{sc} (mA/cm^2) quickly rises with increasing absorber layer thickness. Wide thickness promotes higher production of electron and hole pairs because it permits significant optical absorption [18]. On the other hand, as the absorber layer's thickness rises, V_{oc} (V) and FF (%) fall. V_{oc} decreases from 1.51V to 1.43V as thickness increases. Jsc increases from 7.02mA/cm2 to 12.95mA/cm^2. FF decreases from 88.68% to 79.16%. Accumulation of charge carriers, carrier recombination increases, Hence, V_{oc} gets decreases. It also affects the FF and PCE reported by many studies [19], [20] and [21].

Thus, best performance of cell efficiency occurs at 800nm with maximum PCE of 14.69%, V_{oc} = 1.44V, J_{sc} = 12.62mA/cm^2 and FF = 80.80%.

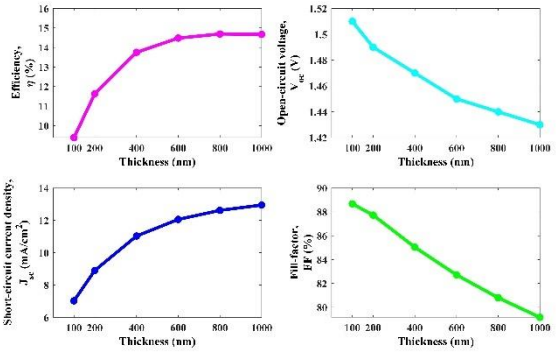

Figure 2: Effect of thickness variation on different electrical parameters of absorber layer

4.1.2 Effect of Thickness variation on Transport layers

To optimize the effect of thickness variation, within the range of 100nm to 1000nm on HTL. first, the thickness of ETL, the absorber layer, and interface layer fix at 100nm, 500nm, and 100nm, respectively. And after this, the performance of cell electrical parameters is observed. From Figure 3(a), the PCE and J_{sc} increase gradually as the thickness of HTL increases. FF of HTL decreases slowly from 83.84% to 83.66% as the thickness of HTL increases. V_{oc} is unaffected within the increasing range of thickness variation. J_{sc} increases from 11.58mA/cm^2 to 11.97mA/cm^2 and PCE increases from 14.16% to 14.51% as the thickness of HTL increases. Thus, the highest PCE of 14.61% for HTL occurs at 1000nm with V_{oc} = 1.46, J_{sc} = 11.97mA/cm^2 and FF = 83.66%. Moreover, to optimize the effect of thickness variation on ETL within the range of 100nm to 1000nm, first, the thickness of HTL, Absorber layer and an interface layer is fixed at 150nm, 500nm and 100nm, respectively. And then performance parameter of the cell is observed. Figure 3(b), shows that PCE decreases continuously from 14.22% to 13.41%. J_{sc} decreases gradually from 11.63mA/cm^2 to 10.98mA/cm^2 as thickness increases causing a high series resistance and absorber losses [22]. FF and V_{oc}

are almost unaffected by the increasing thickness of the ETL. Thus, the highest PCE of 14.22% at 100nm thickness with V_{oc} = 1.46V, J_{sc} = 21.63mA/cm^2 and FF = 83.82%.

Finally, by observing the impact of thickness variation on both the transport layers and the absorber layer, it can determine that the cell performance parameters for the impact of thickness variation on the absorber layer are more prominent than the impact of thickness variation on the absorber layer.

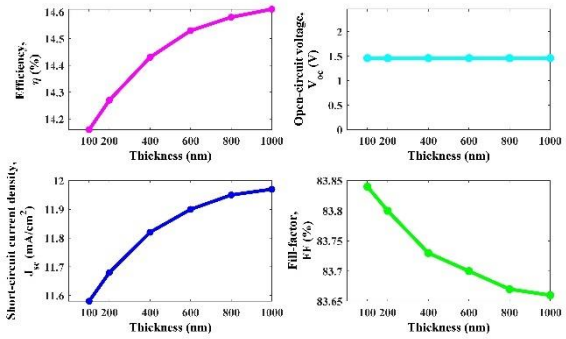

(a)

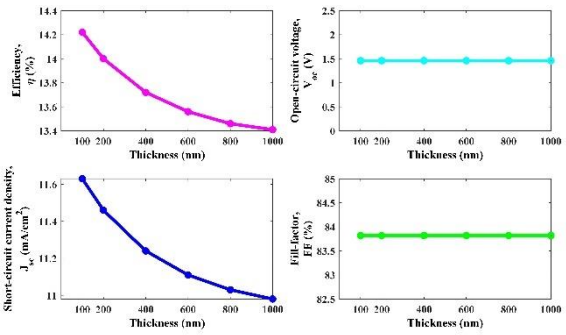

(b)

Figure 3: (a) Effect of Thickness variation on different electrical parameters of HTL and (b) Thickness variation on different electrical parameters of ETL

4.1.3 Effect of Thickness variation on Interface layer (n-3C-SiC)

To optimize the effect of thickness variation on the interface layer. Within the range of 100nm to 1000nm. The first thickness of HTL, Absorber layer, and ETL was fixed at 150nm, 500nm, and 100nm, respectively. Then the thickness variation effect can be investigated. Figure 4 shows that both J_{sc} and PCE increases continuously as the thickness of the interface layer increases from 100nm to 600nm. Beyond 600nm, both the electrical parameters start decaying. V_{oc} slightly increases only from 400nm to 600nm. Besides this thickness range V_{oc} is unaffected by thickness variation. FF starts increasing continuously as thickness increases. Thus, optimized electrical parameters with the highest PCE of 14.57% at 600nm with V_{oc} = 1.47V, J_{sc} = 11.70mA/cm^2 and FF = 84.94%.

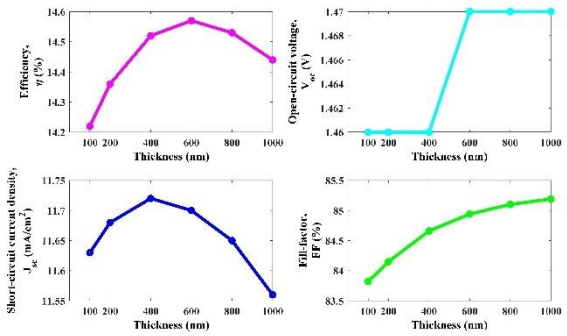

Figure 4: Effect of thickness variation on different parameters of interface layer

4.2 Doping Density Optimization of The Modified Model

4.2.1 Effect of Acceptor Doping concentration variation on Absorber layer ($Cs_3Bi_2I_9$)

To optimize the effect of acceptor doping concentration (N_A) on the absorber layer within the range of 1×10^{15}/cm^3 to 1×10^{22}/cm^3, the first doping concentration of HTL, interface layer, and ETL fixed at N_A = 1×10^{18}/cm^3, N_D = 1×10^{18}/cm^3 and N_D = 1×10^{19}/cm^3 respectively. Then all electrical parameters are calculated.

From Figure 5(a), an adverse sharp decrement in PCE and J_{sc} is observed as the absorber layer's N_A increases initially, from 1×10^{15}/cm^3 to 1×10^{16}/cm^3, a very slow decrement is seen in PCE and J_{sc} almost unaffected within this point of value. PCE decreases from 14.26% to 3.11% and J_{sc} decreases from 11.63mA/cm^2 to 2.10mA/cm^2 as N_A doping concentration increases. The reason behind decay is a reduction in the depletion width of the absorber layer as N_A rises, which enhances the recombination process [23]. On the other hand, from Figure 5(b), Both FF and V_{oc} rise continuously as doping concentration increases. V_{oc} increases from 1.46V to 1.62V and FF from 83.79% to 91.81%.

Thus, optimized electrical parameter with the highest PCE of 14.26% at N_A = 1×10^{15}/cm^3 with V_{oc}= 1.46V, J_{sc} = 11.63mA/cm^2 and FF = 83.79%.

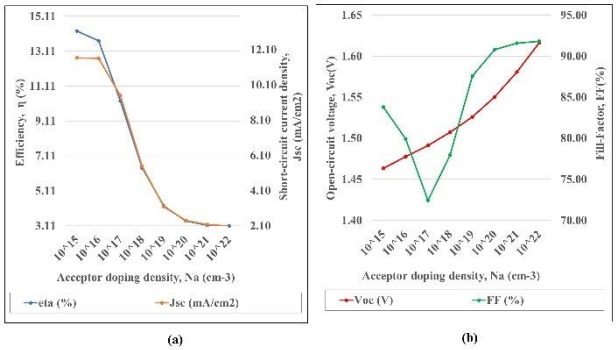

Figure 5: Effect of acceptor doping concentration on different electrical parameters of absorber layer

4.2.2 Effect of Doping concentration variation on Transport layers

To optimize the effect of Acceptor doping density (N_A) of HTL within the range of 1×10^{15} to $1\times10^{22}/cm^3$, the first doping concentration of absorber layer, interface layer, and ETL fixed at $1\times10^{9}/cm^3$, $1\times10^{18}/cm^3$ and $1\times10^{19}/cm^3$ then all electrical parameters will be calculated. Due to the rise in N_A, J_{sc} and FF increases because of the resistance of HTL decay, by rising in hole mobility as N_A rises [24], [25]. To increases the potential used to separate the excitons and reduces the recombination rate, it becomes necessary to enhance the electric field between HTL and ETL as N_A increases [26]. From Figure 6(a), the Jsc of HTL decreases gradually from 11.79mA/cm^2 to 11.48mA/cm^2 as N_A increases. Initially, PCE of HTL increases sharply after the value of $N_A = 1\times10^{19}/cm^3$, PCE decreases slowly. From Figure 6(b), V_{oc} shows slight increment till $N_A = 1\times10^{17}/cm^3$, After this value, V_{oc} becomes unaffected as N_A increases. However, N_A increases from 79.77mA/cm^2 to 84.04mA/cm^2, a sharp increment noticed in the FF of HTL.

Thus, optimized electrical parameter for HTL, highest PCE of 14.24% at $N_A = 1\times10^{19}/cm^3$ with V_{oc} = 1.46V, J_{sc} = 11.62mA/cm^2 and FF = 83.93%.

To optimize the Donor doping density (N_D) of ETL within the range of 1×10^{15} to $1\times10^{22}/cm^3$. The first doping concentration of HTL, the absorber layer, an interface layer fixed at $N_A = 1\times10^{18}/cm^3$, $1\times10^{9}/cm^3$, and $1\times10^{18}/cm^3$. Then, all electrical parameters will be analyzed. From Figure 7(a), J_{sc} and PCE decay slowly as N_D of ETL increases. J_{sc} decreases from 11.65mA/cm^2 to 11.63mA/cm^2 and PCE decreases 14.24% to 14.21%. from Figure 7(b), it can figure out that V_{oc} and FF almost unaffected by increasing N_D of ETL.

Thus, optimized electrical parameter having highest PCE of 14.24% at $N_D = 1\times10^{15}/cm^3$ with V_{oc} = 1.46V, J_{sc} = 11.65mA/cm^2 and FF = 83.81%.

Finally, it can be said that the influence of changing the doping concentration in transport layers (HTL and ETL) is less significant than the impact of changing the doping concentration in the absorber layer on the performance parameters of the cell.

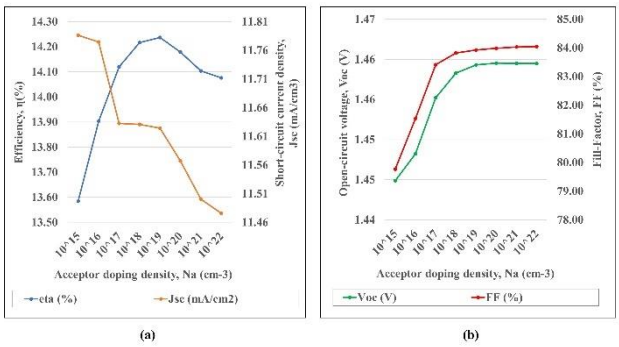

Figure 6: Effect of acceptor doping concentration variation on different electrical parameters of HTL

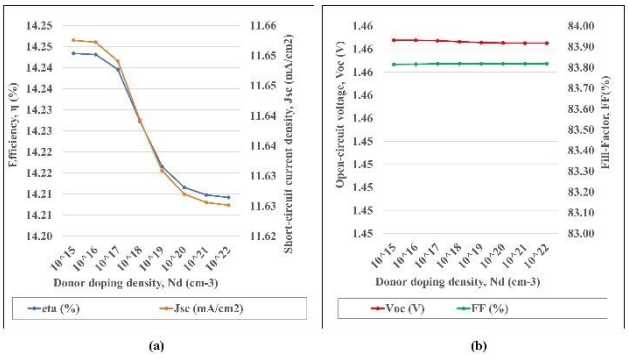

Figure 7: Effect of donor doping concentration variation on different electrical parameters of ETL

4.2.3 Effect of Donor Doping concentration variation on interface layer (n-3C-SiC)

To optimize the impact of donor doping concentration (N_D) variation on interface layer, Within the range of 1×10^{15} to $1\times10^{22}/cm^3$. The first doping concentration of HTL, absorber layer and ETL is fixed at $1\times10^{18}/cm^3$, $1\times10^{9}/cm^3$ and $1\times10^{19}/cm^3$ respectively. Then all electrical parameters are calculated.

From Figure 8(a), J_{sc} is unaffected as N_D of interface layer increases. PCE rises continuously from 12.96% to 14.66% till the value of N_D reaches to $1\times10^{9}/cm^3$ and beyond this value PCE starts decaying.

From Figure 8(b), it can be noticed that from N_D = 1×10^{15} to 1×10^{18}/cm3, V_{oc} does not affect by doping variation, but beyond this value, V_{oc} starts decaying. FF increases continuously from 76.29% to 86.67% as the N_D reaches 1×10^{15} to 1×10^{19}/cm^3, beyond this concentration FF decays.

Thus, optimized electrical parameters having highest PCE of 14.66% at N_D = 1×10^{19}/cm^3 with V_{oc} = 1.45V, J_{sc} = 11.63mA/cm^2 and FF = 86.67%.

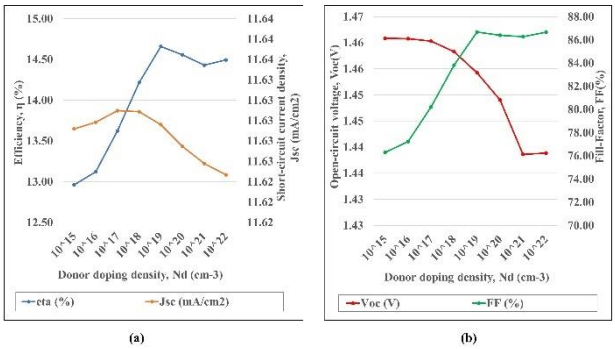

Figure 8: Effect of donor doping concentration on different electrical parameters of interface layer

5 Optimized Performance Parameters of Modified Device Structure

Finally, optimized electrical performance parameters for their optimized cell input parameter for modified structure Au/$Cs_3Bi_2I_9$/n-3C-SiC/TiO_2/TCO, having most optimum value of thickness and doping concentration of each layer listed in **Table 5**. Further, by considering all these values, the modified structure is simulated to figure out the highest PCE. J-V characteristics of modified structure can be analyzed in Figure 9, Which clearly shows an improvement in the short-circuit current density of the initial and optimized cell structure. In **Table 6**, optimized electrical performance parameters of the modified structure show an improvement in J_{sc}, FF, PCE and unaffected V_{oc} value. Hence, highest PCE of 15.63% with V_{oc} = 1.45V, J_{sc} = 12.60mA/cm^2 and FF = 85.52%.

Table 5

optimized photovoltaic input parameters of each layer of modified structure Au/Cu_2O/$Cs_3Bi_2I_9$/n-3C-SiC/TiO_2/TCO observed from series of simulation

Modiied Solar Cell layers	Thickness (nm)	Acceptor Doping Density N_A (cm^{-3})	Donor Doping Density N_D (cm^{-3})
Cu_2O	1000	1×10^{19}	0
$Cs_3Bi_2I_9$	800	1×10^{15}	1×10^{9}
n-3C-SiC	600	0	1×10^{19}
TiO_2	100	0	1×10^{15}

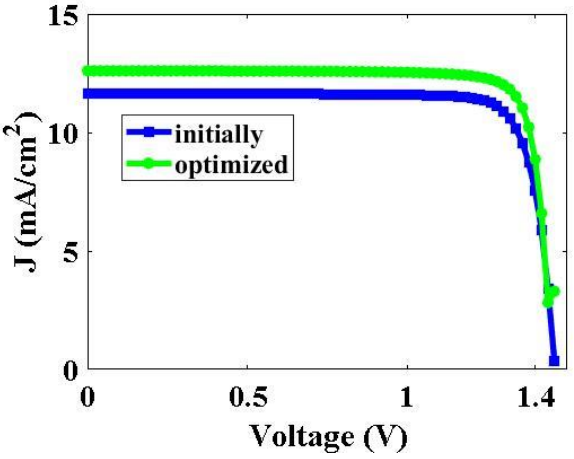

Figure 9: J-V characteristics of modified structure

Table 6

Optimized performance parameters of modified structure Au/Cu_2O/$Cs_3Bi_2I_9$/n-3C-SiC/TiO_2/TCO observed from series of simulation

Electrical performance parameter	Modified cell structure	
	Initially	Optimized
Voc (V)	1.45	1.45
Jsc (mA/cm^2)	11.63	12.60
FF (%)	83.82	85.52
Eta (%)	14.22	15.63

6 Conclusion

In this study, First, a lead-free bismuth-based perovskite solar cell is designed according to the available literature information. Then a simulation study is performed with this structure having defects, which shows decay in the performance parameters of the cell. Moreover, the suggested device structure, which have defects, has an interface layer of n-3C-SiC inserted between the absorber layer and electron transport layer to increase the power conversion efficiency. Which increases the PCE from 13.39% to 14.22 %. Further, to optimize the performance of the cell parameter of this modified structure Au/Cu_2O/$Cs_3Bi_2I_9$/n-3C-SiC/TiO_2/TCO, variation of thickness and doping concentration of each layer is investigated. After the investigation, it is found that the thickness and doping concentration variation effect plays a crucial role in maximizing the cell performance parameters. Last but not least, by

simulating the modified structure again while maintaining all these optimum values for the thickness and doping concentration of each layer, the results indicate V_{oc} = 1.45V, J_{sc} =12.60mA/cm^2, FF= 85.52%, and highest PCE = 15.63%. Therefore, this study tells that PCE can be enhanced by inserting an interface layer and optimizing each layer's thickness and doping concentration. Finally, the presented study sheds the light on the lead-free bismuth-based perovskite solar cell with an interface layer between the absorber layer and ETL. As a result, this research will contribute to the understanding of the highly efficient and stable lead-free bismuth-based perovskite solar cell and pave the way for the advancement of lead-free photovoltaic devices.

7 Acknowledgment

Author would like to thank Honorary Professor Dr. Marc Burgelman and his team, University of Gent, Belgium, department of Electronics and Information Systems (ELIS) for providing the SCAPS-1D simulation software package on request.

8 References

[1] M. A. Green, A. H. Baillie and H. J. Snaith, "The emergence of perovskite solar cells," Nature photonics, vol. 8, pp. 506-514, 2014.

[2] B. R. C. E. Photovoltaic Research, "NREL Transforming Energy," [Online]. Available: https://www.nrel.gov/pv/cell-efficiency.html/.

[3] M. Lyu, J.-H. Yun, P. Chen, M. Hao and L. Wang, "Addressing toxicity of lead: progress and applications of low-toxic metal halide perovskites and their derivatives," Advanced Energy Materials, vol. 7, p. 1602512, 2017.

[4] P. V. Kamat, J. Bisquert and J. Buriak, "Lead-Free Perovskite Solar Cells," ACS Energy Letters, vol. 2, pp. 904-905, 2017.

[5] M. Wang, P. Cheng, S. Bai, J. Gu, F. Li, Z. Yang and M. Liu, "High-quality sequential-vapor-deposited Cs2AgBiBr6 thin films for lead-free perovskite solar cells," Solar Rrl, vol. 12, p. 1800217, 2018.

[6] B. W. Park, B. Philippe, X. Zhang, H. Rensmo, G. Boschloo and E. M. J. Johansson, "Bismuth based hybrid perovskites A3Bi2I9 (A: methylammonium or cesium) for solar cell application," Advanced materials, vol. 27, pp. 6806-6813, 2015.

[7] R. Waykar, A. Bhorde, S. Nair, S. Pandharkar, B. Gabhale, R. Aher, S. Rondiya, A. Waghmare, A. Punde, P. Vairale, M. Prasad and S. Jadkar, "Environmentally stable lead-free cesium bismuth iodide (Cs3Bi2I9) perovskite: Synthesis to solar cell application," Journal of Physics and Chemistry of Solids, vol. 146, p. 109608, 2020.

[8] F. Bai, Y. Hu, Y. Hu, T. Qiu, X. Miao and S. Zhang, "Lead-free, air-stable ultrathin Cs3Bi2I9 perovskite nanosheets for solar cells," Solar energy materials and solar cells, vol. 184, pp. 15-21, 2018.

[9] Z. Zhang, X. Li, X. Xia, Z. Wang, Z. Huang, B. Lei and Y. Gao, "High-quality (CH3NH3) 3Bi2I9 film-based solar cells: pushing efficiency up to 1.64%," The journal of physical chemistry letters, vol. 8, pp. 4300-4307, 2017.

[10] S. Raghvendra, C. Pathak and S. K. Pandey, "Design, performance, and defect density analysis of efficient eco-friendly perovskite solar cell," IEEE Transactions on Electron Devices, vol. 67(7), pp. 2837-2843, 2020.

[11] M. S. S. Basyoni, M. M. Salah, M. Mousa, A. Shaker, A. Zekry, M. Abouelatta, M. T. Alshammari, K. A. Al-Dhlan and C. Gontrand, "On the Investigation of Interface Defects of Solar Cells: Lead-Based vs Lead-Free Perovskite," IEEE Access, vol. 9, pp. 130221-130232, 2021.

[12] Y. He, L. Xu, C. Yang, X. Guo and S. Li, "Design and numerical investigation of a lead-free inorganic layered double perovskite Cs4CuSb2Cl12 nanocrystal solar cell by SCAPS-1D," Nanomaterials, vol. 11, p. 2321, 2021.

[13] S. Ahmed, F. Jannat and M. A. Alim, "A study of Cesium Titanium Bromide based perovskite solar cell with different Hole and Electron transport materials," in IEEE, Dhaka, Bangladesh, 2020.

[14] D. N. Q. Agha and Q. T. Algwari, "The influence of the interface layer between the electron transport layer and absorber on the performance of perovskite solar cells," In IOP Conference Series: Materials Science and Engineering, vol. 1152, p. 012033, 2021.

[15] M. T. Islam, M. R. Jani, K. M. Shorowordi, Z. Hoque, A. M. Gokcek, V. Vattipally, S. S. Nishat and S. Ahmed, "Numerical simulation studies of Cs3Bi2I9 perovskite solar device with optimal selection of electron and hole transport layers," Optik, vol. 231, p. 166417, 2021.

[16] M. Burgelman, P. Nollet and S. Degrave, "Modelling polycrystalline semiconductor solar cells," Thin solid films, vol. 361, pp. 527-532, 2000.

[17] J. Verschraegen and M. Burgelman, "Numerical modeling of intra-band tunneling for heterojunction solar cells in SCAPS," Thin Solid Films, vol. 515(15), pp. 6276-6279, 2007.

[18] S. A. Moiz, A. N. M. Alahmadi and A. J. Aljohani, "Design of a Novel Lead-Free Perovskite Solar Cell for 17.83% Efficiency," IEEE Access, vol. 9, pp. 54254-54263, 2021.

[19] P. Wang, Y. Zhao and T. Wang, "Recent progress and prospects of integrated perovskite/organic solar cells," Applied Physics Reviews, vol. 7, p. 031303, 2020.

[20] M. Daboczi, I. Hamilton, S. Xu, J. Luke, S. Limbu, J. Lee, M. A. McLachlan, K. Lee, J. R. Durrant, I. D. Baikie and J.-S. Kim, "Origin of open-circuit voltage losses in perovskite solar cells investigated by surface photovoltage measurement," ACS applied materials & interfaces, vol. 11, pp. 46808-46817, 2019.

[21] M. Daboczi, J. Kim, J. Lee, H. Kang, I. Hamilton, C.-T. Lin, S. D. Dimitrov, M. A. McLachlan, K. Lee, J. R. Durrant and J.-S. Kim, "Towards efficient integrated perovskite/organic bulk heterojunction solar cells: Interfacial energetic requirement to reduce charge carrier recombination losses," Advanced Functional Materials, vol. 30(25), p. 2001482, 2020.

[22] R. Jeyakumar, A. Bag, R. Nekovei and R. Radhakrishnan, "Influence of electron transport layer (TiO2) thickness and its doping density on the performance of CH3NH3PbI3-based planar perovskite solar cells," Journal of Electronic Materials, vol. 49(6), pp. 3533-3539, 2020.

[23] Y. An, A. Shang, G. Cao, S. Wu, D. Ma and X. Li, "Perovskite solar cells: optoelectronic simulation and optimization," Solar RRL, vol. 2(11), p. 1800126, 2018.

[24] A. Abate, T. Leijtens, S. Pathak, J. Teuscher, R. Avolio, M. E. Errico, J. Krikpatrik, J. M. Ball, P. Docampo, I. McPherson and H. J. Snaith, "Lithium salts as “redox active” p-type dopants for organic semiconductors and their impact in solid-state dye-sensitized solar cells," Physical Chemistry Chemical Physics, vol. 15(7), pp. 2572-2579, 2013.

[25] T. Leijtens, J. Lim, J. Teuscher, T. Park and H. J. Snaith, "Charge density dependent mobility of organic hole-transporters and mesoporous TiO2 determined by transient mobility spectroscopy: implications to dye-sensitized and organic solar cells," Advanced Materials, vol. 25(23), pp. 3227-3233, 2013.

[26] V. A. Trukhanov, V. V. Bruevich and D. Y. Paraschuk, "Effect of doping on performance of organic solar cells," Physical Review B, vol. 84(20), p. 205318, 2011.